The Meteoritical Society

Meteoritics & Planetary Science 44, Nr 2, 187–199 (2009)
Abstract available online at http://meteoritics.org

The Twannberg (Switzerland) IIG iron meteorites: Mineralogy, chemistry, and CRE ages

Beda A. HOFMANN[1*], Silvio LORENZETTI[2, 3], Otto EUGSTER[2], Urs KRÄHENBÜHL[4], Gregory HERZOG[5], Feride SEREFIDDIN[5, 6], Edwin GNOS[7, 8], Manuel EGGIMANN[1, 7], and John T. WASSON[9]

[1]Naturhistorisches Museum der Burgergemeinde Bern, Bernastrasse 15, CH-3005 Bern, Switzerland
[2]Physikalisches Institut, Abteilung für Weltraumforschung und Planetologie, Sidlerstr. 5, CH-3012 Bern, Switzerland
[3]Present address: Institut für Biomechanik, ETH, CH-8093 Zürich, Switzerland
[4]Abteilung für Chemie und Biochemie, Universität Bern, Freiestr. 3, CH-3012 Bern, Switzerland
[5]Department of Chemistry, Rutgers University, 610 Taylor Rd., Piscataway, New Jersey 08854, USA
[6]Present address: Cuesta College, Highway 1, San Luis Obispo, California 93403, USA
[7]Institute for Geological Sciences, Baltzerstrasse 1–3, CH-3012 Bern, Switzerland
[8]Present address: Musée d'histoire naturelle de la ville de Genève, Geneva, Switzerland
[9]Institute of Geophysics and Planetary Physics, University of California, Los Angeles, California 90095–1567, USA
*Corresponding author. E-mail: beda.hofmann@geo.unibe.ch

(Received 19 April 2008; revision accepted 25 September 2008)

Abstract–The original mass (15915 g) of the Twannberg IIG (low Ni-, high P) iron was found in 1984. Five additional masses (12 to 2488 g) were recovered between 2000 and 2007 in the area. The different masses show identical mineralogy consisting of kamacite single crystals with inclusions of three types of schreibersite crystals: cm-sized skeletal (10.5% Ni), lamellar (17.2% Ni), and 1–3 × 10 µm-sized microprismatic (23.9% Ni). Masses I and II were compared in detail and have virtually identical microstructure, hardness, chemical composition, cosmic-ray exposure (CRE) ages, and ^{10}Be and ^{26}Al activities. Bulk concentrations of 5.2% Ni and 2.0% P were calculated. The preatmospheric mass is estimated to have been at least 11,000 kg. The average CRE age for the different Twannberg samples is 230 ± 50 Ma. Detrital terrestrial mineral grains in the oxide rinds of the three larger masses indicate that they oxidized while they were incorporated in a glacial till deposited by the Rhône glacier during the last glaciation (Würm). The find location of mass I is located at the limit of glaciation where the meteorite may have deposited after transport by the glacier over considerable distance. All evidence indicates pairing of the six masses, which may be part of a larger shower as is indicated by the large inferred pre-atmospheric mass.

INTRODUCTION AND CIRCUMSTANCES OF FINDS

In this work, we present the information about the find circumstances and characteristics of six iron meteorite masses that were collected on the Twann Mt. (Twannberg) and its surroundings, about 28 km northwest of Bern, Switzerland (Table 1). Representative views of the three larger masses are shown in Fig. 1. Mass I was found by Margrit Christen during the removal of stones from a freshly ploughed field on Twannberg (Twann Mt.) near the Gruebmatt farm where it was kept as a curiosity for about a year. It was then reported to the curator of the meteorite collection of the Bally Museum in Schönenwerd, Switzerland, who recognized it as a meteorite and initiated an investigation (Bühler 1986a, 1986b). It was classified as an ungrouped hexahedrite to coarsest octahedrite and was named "Twannberg" (Graham 1986), and is here identified as Twannberg I. The circumstances of the find of Twannberg I and a summary of detailed investigations by several laboratories are given by Bühler (1986b).

Mass II was discovered by Marc Jost in the attic of a 17th century house (built around 1650) in the village of Twann, 3.5 km SW of the find location of Twannberg I. The find was reported to the first author on September 5, 2000, and one day later, the main mass was inspected in Twann and then brought to Bern for further investigation. The exact find locality in the attic was visited by the first author on December 20, 2000, with the finder. This fragment had been placed together with iron utensils on top of a stone wall in the attic inside the house just below the roof. The meteorite had been covered with a thick layer of dust and dust-free area showing the exact position of the

Table 1. Main characteristics of the Twannberg iron meteorite masses.

	Twannberg I	Twannberg II	Twannberg III	Twannberg IV	Twannberg V	Twannberg VI
Date of find or recognition	May 9, 1984	August 2000	September 2, 2005	Summer 2007	Summer 2007	Summer 2007
Place of find	Twannberg, Canton of Bern, Switzerland	Dorfgasse 7,Twann, Canton of Bern, Switzerland	Museum Schwab, Biel, Canton of Bern, Switzerland	Twannbach	Twannbach	Twannbach
Type of find place	Field after plowing	Attic of 17th century house	Old museum collection	River bed	River bed	River bed
Longitude and latitude[1]	47°7.39′N; 7°10.63′E	47°5.73′N; 7°9.45′E	47°8.33′N; 7°14.48′E	47°5.80′N; 7°8.83′E	47°5.80′N; 7°8.83′E	47°5.80′N; 7°8.83′E
Altitude (m)	975	445	440	560	560	560
Finder	Margrit Christen	Marc Jost	Museum Schwab Collection	Marcel Wälti	Daniel Ducrest	Marcel Wälti
Original dimensions	18 ×15 ×12 cm	13 × 9 × 6 cm	12 ×10 × 7 cm	3.3 × 2.4 × 1.6 cm	2.6 × 1.3 × 0.9 cm	2.1 × 1.9 × 1.1 cm
Recovered mass	15,915 g	2246 g	2533 g	~50 g	14.2 g	12.7 g
Main mass as of December 2007	9347 g	1962 g	2487.5 g	48.7 g	12.8 g	12.3 g
NMBE inv. nr.	36,467	35,119	37,777	39,378	39,307	39,308

[1]As determined with GPS, WGS 84 map datum.

meteorite was still clearly visible. This meteorite must have been moved to the attic some time during the last 350 years. The find of this mass triggered a comparison of masses I and II.

Mass III: after the near completion of the study of masses I and II, mass III was discovered in 2005 in a rock collection transferred from the Schwab Museum in Biel to the Natural History Museum Bern (NMBE). This mass was labeled as "Eisenglanz" (hematite) in the handwriting of Fritz Antenen (1867–1944), who reorganized the collection in 1932. It can thus be assumed that this mass was found before 1932, but not recognized as a meteorite.

Masses IV, V, and VI were discovered in the summer of 2007 in the Twannbach canyon a few 100 m NW of Twann by Marcel Wälti while searching for gold, and by Daniel Ducrest while searching for interesting pebbles.

The newly discovered masses are clearly paired (see below) with the original Twannberg mass (TW I) and thus represent additional fragments of the Twannberg fall, bringing the total mass to 20.771 kg. General information on the six masses of Twannberg is given in Table 1. After the discovery of TW II, its finder Marc Jost searched the Twannberg area for more than 100 hours using a metal detector, but found no more meteorites.

After its discovery, Twannberg I was hosted in the Bally Museum, Schönenwerd, Switzerland, from 1985 until 2002 when it was acquired by NMBE on the dissolution of the Bally Museum collection. Twannberg II was acquired from the finder by NMBE in 2000. Twannberg III is at NMBE as a permanent loan from the Museum Schwab. Masses IV to VI are in private collections, with small samples being deposited at NMBE. Because Twannberg has never been fully described in the literature, data are scattered in specialized (Wasson et al. 1989; Schultz and Franke 2004) and popular articles (Bühler 1986a, 1986b, 1988; Hofmann 2005). In this paper, several characteristics of the different masses are discussed and tested for pairing, with special emphasis on masses I and II.

First, the results of the mineralogical and chemical investigations are presented in order to establish the pairing of the masses. Based on the conclusions concerning mineralogy, chemistry, and cosmic-ray exposure history, it will be shown that Twannberg I and II are two fragments of the same meteorite fall. Twannberg III–VI have been investigated in less detail due to their finding during an advanced stage of this study, but the identical and otherwise very rare structure, combined with indications for weathering in a similar environment, clearly indicate pairing as well.

Second, the cosmic-ray exposure (CRE) history will be characterized. The relevance of the determination of CRE ages of iron meteorites was demonstrated by Lavielle et al. (1999) for the question of the constancy of the galactic cosmic ray flux (CRF) during the period of 150–700 Ma before the present. For this time interval, based on the average ^{36}Cl or ^{36}Ar production rates, these authors found a 28% lower CRF when compared to production rates commonly used for the recent CRF.

Twannberg is a member of iron meteorite group IIG. With the classification of Twannberg in 1986 and Guanaco in 2001 as IIG meteorites, the minimum population (5) for group designation was reached, and the grouplet once known as the Bellsbank trio became group IIG. All of these meteorites are hexahedrites being very low in nickel (4.1 to 4.9% Ni in metal) and high in P, leading to characteristic large inclusions of skeletal schreibersite $(Fe,Ni)_3P$.

REGIONAL CONTEXT AND GEOLOGY

Twannberg I was found on top of the Twannberg, at an altitude of 975 m. Twannberg is the southernmost anticlinal fold of the SW-NE-trending Jura mountain chain of Pliocene age. The mountains consists of Upper Jurassic (Tithonian) to Lower Cretaceous (Valanginian) limestones and minor marls and are partially covered by up to several meters of Quaternary glacial till (Schär et al. 1971), resulting in an

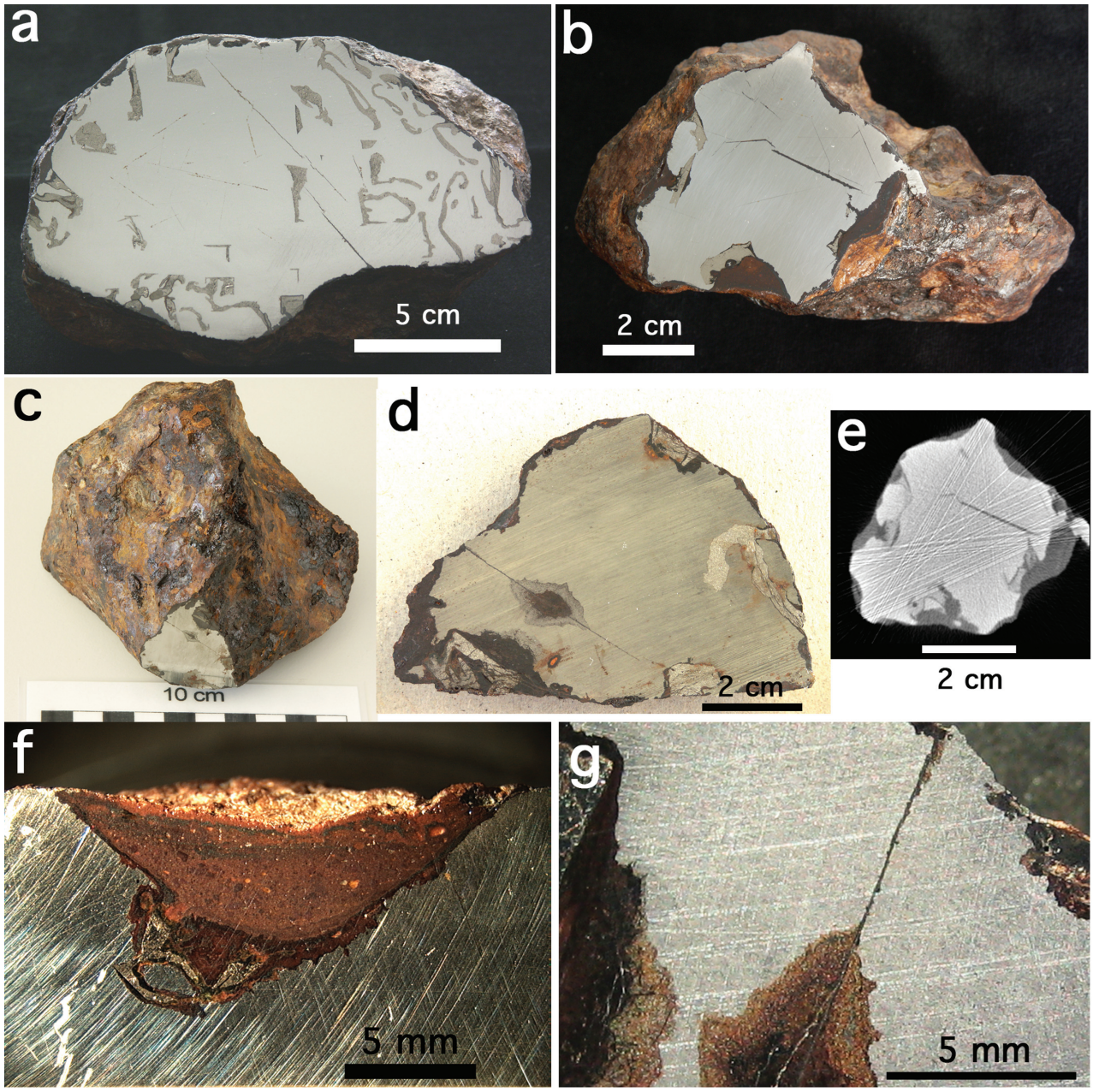

Fig. 1. Macroscopic features of the three largest Twannberg masses. a) Section across Twannberg I displaying large skeletal schreibersite inclusions and fissures following lamellar schreibersites oriented in up to 10 directions. b) Section across Twannberg II containing skeletal schreibersite and fractures associated with lamellar schreibersite (7 directions). Note rinds of oxides and oxide-impregnated till of irregular thickness. c) Twannberg III showing particularly strong effects of terrestrial oxidation. d) Section of Twannberg III showing skeletal schreibersites and oxidation halo (partial oxidation of kamacite) on schreibersite-induced fracture. e) X-ray tomograph of Twannberg II, located about 5 mm below the section shown in (b). Kamacite (light grey), schreibersite (medium grey), and oxide rind (dark grey) are clearly distinguishable. White lines are artifacts from the tomography process. f) Embayment in Twannberg II with adhering glacial till impregnated with iron hydroxides. g) Detail of Twannberg III (same section as d) after etching, displaying various sets of Neumann bands.

abundance of scattered pebbles and blocks of crystalline and sedimentary rocks. This debris was transported by the Rhône glacier from the Alps over a distance of 100 to 250 km. The find location of Twannberg I is close to the northern maximal extension of the Rhône glacier during the last (Würm) ice age (Fig. 2). The village of Twann, where TWII was found in a house, is located on the NW shore of the Lake of Biel, at an altitude of 430 m, among local outcrops of Cretaceous limestone and glacial till. Twann is located at the boundary between the Jura fold belt and the Tertiary molasse basin (Swiss plateau) to the SW. The area is covered by vineyards at low elevations wherever the hillsides face S-SE, but is

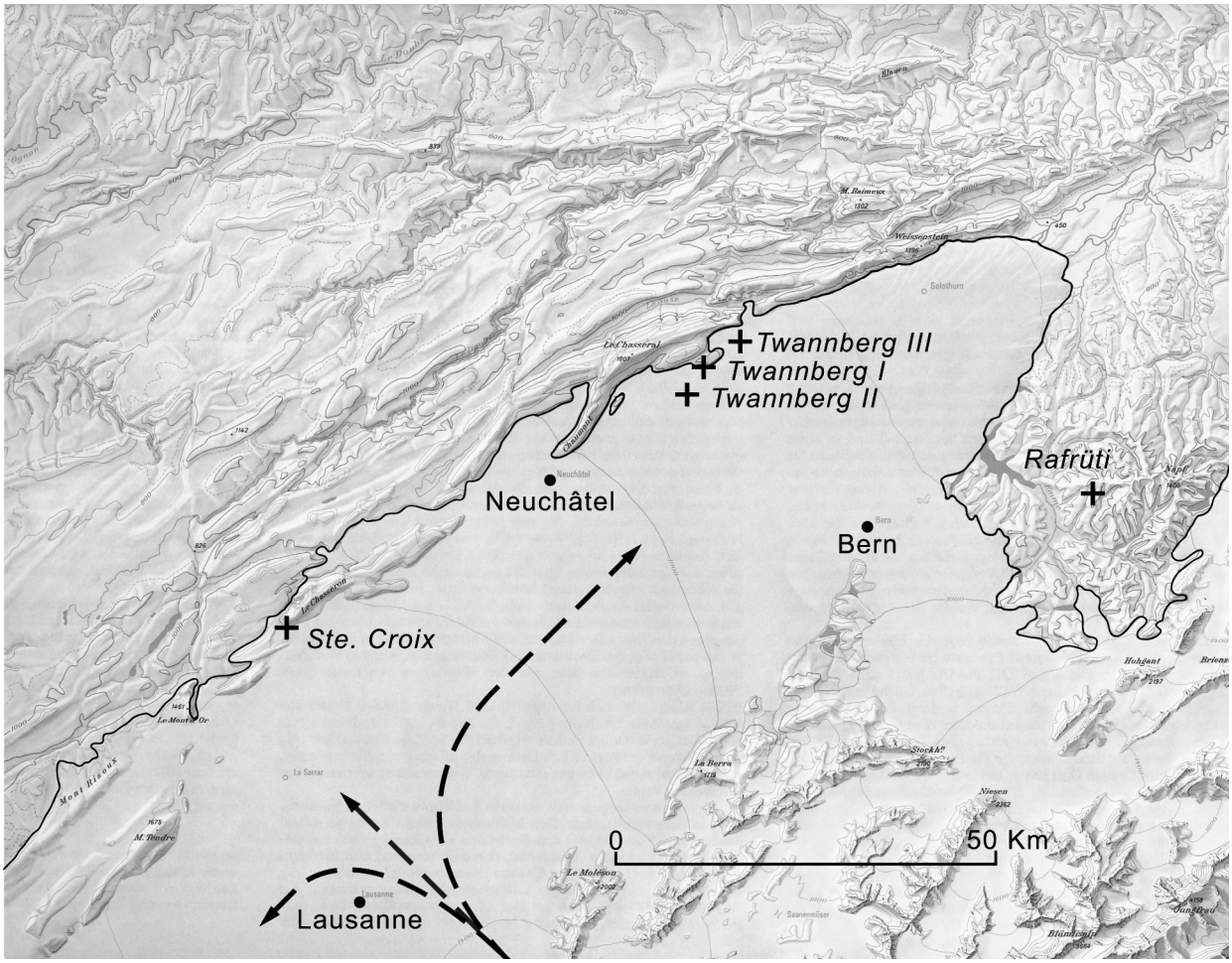

Fig. 2. Maximum extension of the Rhône glacier during the last (Würm) ice age (after Jäckli 1970) in the northern foreland of the Alps. Marked are the find locations of the Twannberg iron meteorites I–III. Find locations of masses IV–VI are identical to II at this scale. Also shown are the find location of the other two Swiss iron meteorites Ste Croix (IIIAB) and Rafrüti (anomalous). Arrows show main flow lines of the Rhône glacier. Both Twannberg and St. Croix were found close to the edge of the ice at its maximum extent.

dominated by forest on the higher slopes. Relatively flat areas at higher elevations on Twannberg are partly forested and partly agricultural land. The city of Biel with museum Schwab, where mass III was discovered, is located at the northeastern end of the Lake of Biel, 8 km NE of Twann. The (secondary) find places of TWII and III are just 3.5 and 5 km from that of TW I. The shores of the Lake of Biel have been inhabited since at least 4000 B.C. Abundant Neolithic artifacts were recovered at Twann and other sites nearby. Reports of rusted masses found in these Neolithic sites were checked, but all evidence indicates that they were due to oxidized pyrite used to make fire.

EXPERIMENTAL PROCEDURES

Bulk Characteristics and Mineralogy

The mineralogy of Twannberg I and II was studied on polished sections using optical microscopy. Hardness measurements were carried out using a Leitz Durimet hardness microscope with a load of 100 g. The volume proportion of schreibersite was determined from an image of a large section of Twannberg I and from several X-ray tomographic images of Twannberg II processed by using image analysis software (NIH image, see below). Troilite abundance was estimated from reflected light microphotographs. Mineral compositions were determined by electron microprobe analysis using a JEOL JXA 8200 instrument with the following analytical conditions: 15 kV, 20 nA, 2 μm beam diameter on sample, K X-ray lines, and $\phi(\rho Z)$ matrix correction. The standards used included metallic Fe, Co and Ni, Cu_3PS_4 (S), Cr_2O_3 (Cr), $FeTiO_3$ (Ti), almandine (Si, Al), and fluorapatite (P). Additional mineral compositional analyses were obtained by standardless EDS analysis using a CamScan CS4 SEM. The mineralogical composition of the oxidation rind was determined by X-ray diffraction (XRD) using a Guinier-De Wolff camera and Fe-radiation. A Zeiss Evo 50 scanning electron microscope

operated at 20 kV, coupled with an energy dispersive system (EDS) was used to perform spot analyses. X-ray tomographs were obtained at EMPA Dübendorf, Switzerland, using an industrial CT scanner operated at 400 kV, 2.25 mA with linear array detectors and a detector aperture of 0.25 × 0.5 mm. Pixel size was 0.25 mm.

Elemental Composition

The fragments of the meteorites taken for the chemical analysis by inductively coupled plasma spectroscopy were cleaned by acid leaching prior to dissolution. Leaching was performed by submerging the whole fragments of the meteorites to be analyzed into a solution of 1.5 M HNO_3 for 90 seconds. Of the fragments 0.25% and 1.2% of their mass, respectively, were dissolved by this procedure. The masses remaining after leaching—typically 0.2 g—along with HNO_3 and H_2O_2 were placed in Teflon pressure bombs and heated with microwave excitation. The concentrations of Fe, Ni, Co, and 10 trace elements in the resulting solutions were measured by ICP-OES or by Quadrupole ICP-MS. Instrumental neutron activation analysis was carried out using protocols described elsewhere (e.g., Wasson and Choi 2004). Duplicate samples of TW I and TW II were studied in separate irradiations. Meteorite bulk compositions were calculated from schreibersite modes, mineral compositions and mineral densities. The minerals considered were mean bulk metal, skeletal schreibersite and a small amount of troilite (0.14% of volume of skeletal schreibersites, based on volume estimate from photomicrographs). A bulk metal P content of 0.34% was adopted, as this is the lower of two bulk measurements (assuming no contamination from skeletal schreibersite).

Noble Gases

Noble gas analyses of samples of about 0.1 g were performed at the Physics Institute of the University of Bern. The samples were heated in vacuum at 90 °C for several days in the storage arm of the extraction system to reduce adsorbed atmospheric gases. The Mo crucible of the extraction system was preconditioned by melting about 0.5 g of stone meteorite material to avoid the reaction of meteoritic Fe,Ni with the Mo of the crucible. This pretreatment was also used to check the proper functioning of the total analytical system. Gases were extracted by RF-heating in a single step at 1700 °C. Completeness of the gas release was checked by adding a final extraction step at 1740 °C. The mass spectrometric analyses and background corrections were performed according to the description by Eugster et al. (1993) using system B. The following blanks were subtracted (units of 10^{-8} cm^3 STP/g): ^{3}He = <0.00004, ^{4}He = 0.04, ^{20}Ne = 0.0008, ^{40}Ar = 0.4. The errors correspond to a 95% confidence level.

Cosmogenic Radionuclides

The Twannberg samples analyzed for cosmogenic radionuclides were dissolved in mineral acids after the addition Al, Be, and/or Cl carriers. Al, Be, and Cl were separated by standard methods (Vogt and Herpers 1988). ^{10}Be/^{9}Be, ^{26}Al/^{27}Al, and ^{36}Cl/Cl isotope ratios for the Twannberg samples were measured by accelerator mass spectrometry (AMS) at Purdue University. The ^{26}Al/^{27}Al and ^{36}Cl/Cl ratios were converted to ^{26}Al and ^{36}Cl activities, respectively using Purdue's in-house standards for ^{26}Al ($t_{1/2}$ = 0.7 Ma) and ^{36}Cl ($t_{1/2}$ = 0.3 Ma). Details of procedures and standards are reported in Vogt et al. (1994). For ^{10}Be ($t_{1/2}$ = 1.5 Ma) the ^{10}Be/^{9}Be ratio was converted to a ^{10}Be activity by using the measured ^{10}Be/^{9}Be ratio of Dhurmsala material prepared by Rolf Michel, and an activity of 22 ± 1 dpm/kg for that material.

RESULTS

Morphology and Mineralogy

Twannberg I originally measured approximately 18 × 15 × 12 cm with a rather isometric shape. Twannberg II has maximum dimensions of 13 × 9 × 6 cm, and mass III of 12 × 10 × 7 cm. The surface of all three large masses is made up of the same type of dark brown oxide rind, up to 6 mm thick locally. Abundant inclusions of grains of quartz, mica and fragments of mica-rich schist are present in the oxide crust of the three masses. The small masses IV to VI were covered by an oxide crust lacking these mineral inclusions, probably because of abrasion during transport in the riverbed.

The mineralogy of Twannberg is simple. Kamacite and schreibersite constitute the majority (99.99%) of the modal composition. We use schreibersite together with a descriptive term for all morphotypes of Fe_3P in this paper. The term "rhabdite" is avoided because this is not an official mineral name and the use has not always been consistent in the literature. Typically the type we call "microprismatic schreibersite," and sometimes also the "lamellar schreibersite," were called "rhabdite." The Twannberg individuals consist of single large kamacite crystals. Neumann bands are common in the kamacite (Fig. 1g). Schreibersite occurs as three types (Fig. 3): Skeletal schreibersite forms crystals up to 4.5 cm long and 2–4 mm wide. These constitute 6–12 vol% of the meteorite. Thin (5–20 μm) lamellar schreibersite having lengths >3.5 cm are found in kamacite (aspect ratio ~1000). The abundance of lamellar schreibersite is relatively low with spacings of at least 1 mm (typically 2–3 mm) between lamellae. Close to skeletal schreibersite, lamellar schreibersite is less common but still present. Microprismatic schreibersite forms 1–3 μm wide and up to 10 m long oriented inclusions in kamacite. Microprismatic schreibersite occurs only at a distance >250 μm

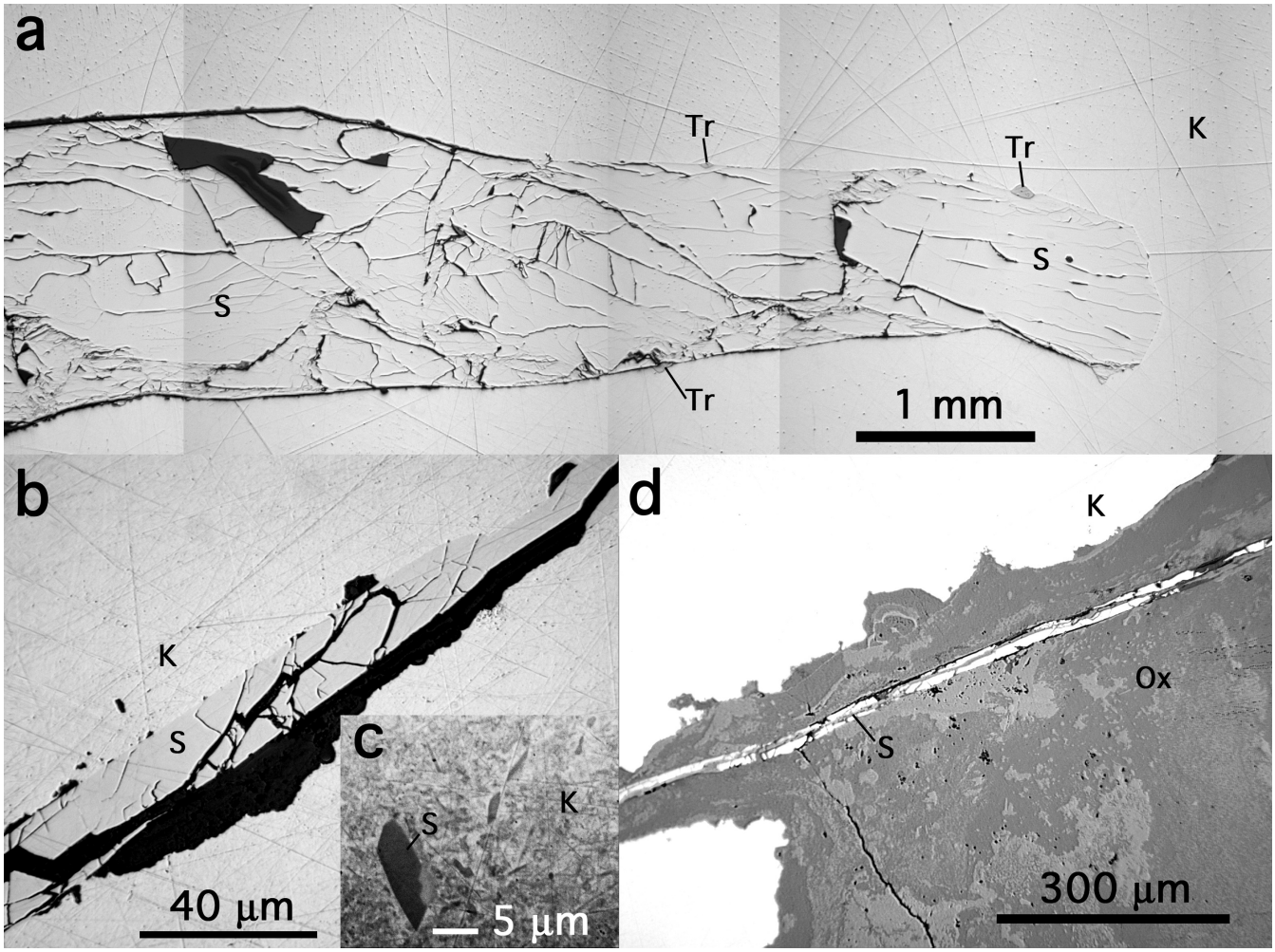

Fig. 3. Types of schreibersite in Twannberg, as observed by reflected light microscopy/SEM. a) Skeletal schreibersite (S) showing brittle fracturing in unfractured kamacite (K). Along the boundary some grains of troilite (Tr) are located. b) Lamellar schreibersite, strongly fractured, in kamacite. Kamacite shows strong alteration in vicinity of fractured schreibersite. Oil immersion. c) BSE image of oriented microprismatic schreibersites in kamacite. Note heterogeneity in kamacite, probably due to microexsolutions of schreibersite. d) Lamellar schreibersite more resistant to weathering than kamacite. Oxidation products (Ox) include magnetite and maghemite (brighter) and darker goethite.

from schreibersite lamellae while kamacite closer to schreibersite lamellae is free of such inclusions. The types of schreibersite observed in Twannberg are very similar to those in other members of group IIE such as Bellsbank (Clarke and Goldstein 1978) and also in hexahedrites with higher bulk Ni (Buchwald 1975; Randich and Goldstein 1978). In Twannberg, the abundance of schreibersite lamellae is lower and the size of microprismatic schreibersites is smaller, however.

Troilite occurs as grains up to 60 µm in size at schreibersite-kamacite grain boundaries and as exsolutions in schreibersite (maximum size 4 × 30 µm). The modal abundance of troilite was estimated relative to schreibersite because troilite was never observed in kamacite. Troilite abundance is 0.14 vol% of skeletal schreibersite, or 0.007–0.014 vol% of the bulk meteorite.

Electron microprobe (EMP) analyses of schreibersite, troilite and kamacite are presented in Table 2. Schreibersite varieties (skeletal crystals, lamellae, and microprisms) are significantly different in terms of their Ni concentrations. The large skeletal schreibersites show the lowest Ni-concentrations (mean 10.47 ± 0.20 wt%). Schreibersite lamellae have an average Ni concentration of 17.15 ± 0.63 wt%. The microprismatic schreibersites, finally, show a mean of 23.9 ± 1.9 wt% Ni. The strong enrichment of Ni in schreibersite relative to kamacite is consistent with results of Randich and Goldstein (1978), Clarke and Goldstein (1978) and Geist et al. (2005). The Ni content in Twannberg schreibersites is considerably lower than that in IIAB hexahedrites, however (~25 to 40 wt% Ni, Randich and Goldstein 1978). The EMP analyses of kamacite show lower Ni (EMP: 3.33, bulk ~4.5 wt%) and Co (EMP: 0.34, bulk 0.5%) than the bulk metal analyses

Table 2. Microprobe analyses of Twannberg phases.

	Skeletal schreibersite		Lamellar schreibersite		Microprismatic schreibersite*		Troilite	Kamacite
	n = 12		n = 5		n = 8		n = 3	n = 11
wt%	mean	±		±		±		
Si	0.01	0	0.01	0.01	n.d.		0.01	0.03
Fe	75.1	0.4	65.4	2.17	60.3	2.7	64.0	97.8
P	15.1	0.01	14.5	1.03	15.4	1.0	0.06	0.14
Al	0.01	0.01	0.01	0.01	n.d.		0.01	0.01
Co	0.06	0.02	0.03	0.01	0.5	0.1	0.18	0.34
Ti	0.01	0.01	<0.01		n.d.		0.02	0.01
Ni	10.5	0.2	17.2	0.63	23.9	1.0	0.33	3.33
S	0.08	0.01	0.02	0.01	n.d.		35.2	0.01
Cr	0.0 ≤ 1	0.01	0.01	0.00	n.d.		0.23	0.01
Total	100.9		97.2		100		100.0	101.7
Normalized for P + S = 1								
Fe	2.75		2.49		2.18		1.04	
Ni	0.36		0.62		0.82		0.01	
Co	0		0		0.02		0	
Cr	0		0				0	
S	0.01		0				1	
P	0.99		1		1		0	

*Standardless EDS analysis on SEM.

(Table 3). For Ni this might be due to the presence of microprismatic schreibersites and Ni-depleted zones in the kamacite near schreibersite, the reason for the low Co remains unclear.

On large cut surfaces, fractures that follow the schreibersite lamellae are quite common (Figs. 1a–d). Fracturing along the brittle schreibersite lamellae resulted in preferred and deep oxidation along lamellar schreibersites. Between 7 (TW II) and up to 10 (TW I) orientations of lamellar schreibersites could be observed, consistent with a complex crystallographic orientation parallel to {221} and possibly {100}. Similar observations have been reported for the hexahedrites North Chile and Coahuila (Buchwald 1975). Based on cut surfaces, the abundance of large schreibersite inclusions was estimated at 12.2 vol% (TW I), 6.0 vol% (TW II) and 9.3 vol% (TW III), similar to the value of 11% obtained by V. Buchwald (in Bühler 1986a, 1986b) on different sections.

Microhardness measurements carried out on kamacite yielded a Vickers hardness of 253 ± 13 (n = 17) for TW I and 240 ± 6 (n = 17) for TW II. Measurements by V. Buchwald (in Bühler 1986a) are identical at 235 ± 15. Schreibersite in TWI has a hardness of 1207 ± 42 (n = 7). The presence of Neumann bands (Fig. 1g) and the kamacite hardness are indicative of medium to strong shock of up to 13 GPa (Buchwald 1975).

The oxidation rinds of TW I and TW II both consist of a mixture of iron oxyhydroxides with mineral grains (mainly quartz, feldspar, mica) derived from the local till (Fig. 1f). Optical microscopy and XRD revealed the presence of goethite, maghemite and magnetite. Locally vivianite $Fe_3(PO_4)_2 \cdot 8H_2O$ was observed in TW II and III in corroded kamacite in contact with schreibersite. In contact with the oxidized rim, schreibersite is clearly more resistant to weathering than kamacite. Oxidation of kamacite in the interior of all Twannberg specimens typically propagates along fractured lamellar schreibersites (Figs. 1d and 3b) and also along skeletal schreibersites. The thickness of the oxidation rind on all masses ranges from 1 to 15 mm, but oxidation along grain boundaries was observed as deep as 30 mm from the surface.

Chemical Composition

Major and trace element contents of Twannberg I and Twannberg II are given in Table 3. With a few exceptions, the respective concentrations in the two samples are identical within the quoted errors. Differences are observed for Ir, Pt, and Re. The higher Ir contents determined by ICP are close to the detection limits; for this element the INAA gives better results (lower by a factor of 2 to 3) and are preferred. For Pt, signals were well above detection limits for both methods and there is no reason to prefer one set of results to the other. For Re, only upper limits are obtained with INAA. The new distinct values for Re based on ICP are compatible with the lower range for octahedrites. Bulk P contents were measured by ICP analysis of cuttings that were taken from a large (17 × 10 cm) section in an attempt to obtain a representative bulk sample. The values of 1.33 wt% P for TW I and 0.34% for TW II likely reflect different losses of brittle schreibersite during sectioning as the values are intermediary between those for kamacite (0.14%, Table 2) and calculated bulk compositions (1.1 to 2.0%, Table 4). Due to the extremely

Table 3. Concentrations of major and trace elements in bulk metal for Twannberg I and II.

Sample	Fe (%)	Ni (%)	Co (ppm)	Cu (ppm)	Ga (ppm)	Ge (ppm)	As (ppm)	Sb (ppm)	W (ppm)	Re (ppm)	Ir (ppm)	Pt (ppm)	Au (ppm)	
Twannberg I[1]		4.42	5210	90	37.9	51.4	17.9	0.163	0.20	<20	0.086	<1.4	1.35	(A)
Twannberg I	95.4	4.31	5120	71	32.0	48	16.9	0.135	0.10	0.01	0.22	0.24	1.05	(B)
Twannberg II		4.50	5220	89	38.4	–	18.1		0.14	<20	0.101	0.9*	1.406	(A)
Twannberg II	95.5	4.79	5170	73	32.5	47	17.6	0.146	0.15	0.012	0.34	0.22	1.04	(B)

[1]Wasson et al. (1989) with one large correction (upper limit sign for Pt) and a few small corrections.
*± 0.6.
A: INAA data.
B: Combined ICP (Fe, Ni, Co, 3% 1σ error) and ICP-MS (remaining elements 10%1σ error).

Table 4. Calculated bulk composition for Twannberg.

Schreibersite (vol%)	TW I 12	TWII 6	TWIII 9.3	TWI* 11
wt%				
Fe	92.4	93.5	92.9	92.4
Ni	5.15	4.83	5.01	5.1
Co	0.47	0.49	0.48	0.50
P	1.95	1.14	1.58	2.00
S	0.01	0.006	0.01	–

*After V. F. Buchwald, in Bühler (1986b).

heterogeneous distribution of brittle schreibersite, the bulk composition of Twannberg is better represented by these calculated values than by the metal analyses. The ratio of Ir in TW II to TW I is ~1.17 ± 0.04 (2σ). The range of Ir concentrations is larger than commonly encountered when separate masses of magmatic iron meteorites are studied.

Cosmogenic Noble Gases

Noble gas data are presented in Table 5. To partition the bulk concentrations into cosmogenic and non-cosmogenic components certain assumptions have to be made: it is assumed that no solar He is present and that the small addition of trapped Ne to the Twannberg II sample is of terrestrial atmospheric origin, as can be judged from the measured $^{20}Ne/^{22}Ne$ ratio in Table 5. The concentration of ^{21}Ne varies among the investigated samples, due, perhaps, to variations in the occurrence of schreibersite $(Fe,Ni)_3P$ inclusions, P being a target element for the production of ^{21}Ne. Our Twannberg I sample shows an enhanced $^{36}Ar/^{38}Ar$ ratio of 1.14 over the purely cosmogenic value of 0.64 (Lavielle et al. 1999). This enhancement is also interpreted as the result of atmospheric contamination, compatible with the presence of pervasive oxidation along schreibersite lamellae. For calculating the cosmogenic ^{38}Ar the terrestrial value for $(^{36}Ar/^{38}Ar)_{tr} = 5.32$ is adopted.

Cosmogenic Radionuclides

Results of the radionuclide analyses appear in Table 6. The ^{10}Be activities are fairly uniform—the total observed variation is less than 10%, which suggests that the samples analyzed came from within a range of (vertical) depths of less than 5 cm or so. This range of depths refers to the last few million years in space. The activities of the cosmogenic radionuclides do not constrain either the lateral distances between samples in space at any time, assuming a more or less spherical meteoroid, or the vertical distances at times greater than a few million years ago. On the other hand, the small mass of the analyzed Twannberg individuals suggests that the samples analyzed were close together for some time.

The ^{10}Be activities are quite low, about 40 times lower than the values of 5–6 dpm/kg typical of small iron meteorites (Fig. 4).

The ^{26}Al activities are also a factor of about 40 lower than the value (3.5 dpm/kg) typical of small iron meteorites. The relative uncertainties of 15–30% are unusually large; they reflect the low measured $^{26}Al/^{27}$ratios, 5–10 × 10^{-14}, which were due in part to low sample activities and in part to the relatively large masses of Al carrier added, ~3 mg. In addition, blank corrections (~1 × 10^{-14}) were appreciable. Although the ^{26}Al activities apparently vary by a factor of two, from 0.056 ± 0.018 to 0.118 ± 0.023, the extreme values differ by only 1.5 ($\sigma_1 + \sigma_2$). In light of the limited range of ^{10}Be activities, it seems likely that either experimental error or differences in composition account for most of the variation in ^{26}Al activities. Twannberg contains 1–2% P along with minor S. Elements other than Fe and Ni with $Z \geq 14$ (Si) contribute appreciably to the production rate of ^{26}Al. In Twannberg, ^{26}Al would probably be produced mainly in schreibersite.

The results for ^{36}Cl scatter appreciably—by a factor of about two. Although production rates of ^{36}Cl from K and Ca are high enough to have caused measurable increases in the ^{36}Cl activities of some samples, unknown analytical problems seem a more likely cause of the observed variations of this radionuclide. The average ^{36}Cl activity for the samples reported in Table 6 is a factor of about 30 lower than found in small iron falls.

DISCUSSION

Geological Environment

The grains of quartz, mica, and mica-rich rock fragments present in the oxide rind of the three large masses clearly indicate that they were in contact with glacial till and not

limestone during weathering. This confirms that TW II and III were originally located in a similar environment as TW I. Given the obvious contact with glacial sediments during weathering, it seems likely that the meteorites were transported by the Rhône glacier and deposited in the till.

Mineralogy

The occurrence of three types of schreibersite reflects crystallization/exsolution under conditions of decreasing temperature. For skeletal schreibersite, a formation temperature of >850 °C was estimated by Doan and Goldstein (1969) and Clarke and Goldstein (1978). These authors argue for an exsolution origin of skeletal schreibersite. We do not exclude a combination of crystallization from melt followed by growth by diffusion of P out of kamacite. Lamellar and microprismatic schreibersites clearly were formed by exsolution. Distances of diffusion for Ni and P can be estimated: In the case of large skeletal schreibersites several mm to cm, in case of schreibersite lamellae ~250 µm (width of zone free of microprismatic schreibersites) and for the microprismatic schreibersites ~10–20 µm (mean spacing divided by 2). The exsolution of schreibersite during cooling caused a redistribution of nickel (and probably of other elements) within the large kamacite crystals and is most likely the reason for the differences observed between bulk metal and microprobe analyses.

The mixture of ductile kamacite with brittle schreibersite present in three very different forms strongly influenced the fracturing pattern of Twannberg. Especially, the very extensive (several cm^2) schreibersite lamellae served as fracturing planes and led to a deep penetration of cracks and, later on, to terrestrial alteration.

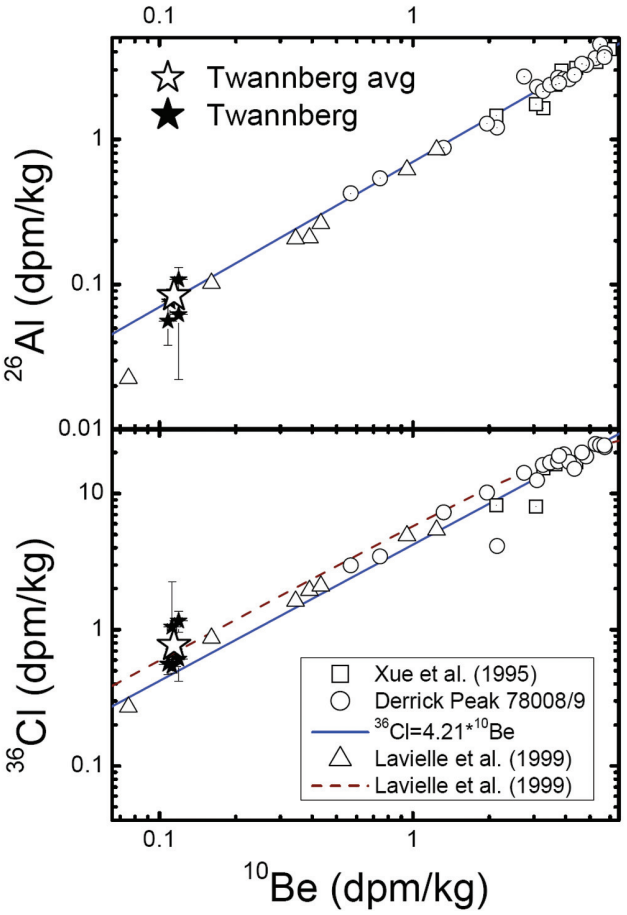

Fig. 4. The activities of ^{36}Cl, ^{26}Al, and ^{10}Be measured in Twannberg samples are lower than but consistent with trends observed for most other iron meteorites. Results for Derrick Peak are from Nishiizumi et al. (1987) after corrections for a terrestrial age of 1 Myr.

Elemental Composition

The two analyzed masses (I and II) are closely similar in composition consistent with derivation from the same parent mass. With a content of 6–12 vol% of schreibersite, it is evident that the chemical analyses, performed on metal-dominated samples, do not properly reflect the bulk composition; skeletal schreibersite was almost entirely excluded from these analyses.

To allow for this, we calculated a bulk composition based on the modal abundance and composition of schreibersite following a procedure used by Buchwald (in Bühler 1986b); this is listed in Table 4. With about 2 wt% P, Twannberg (like the other IIG irons) belongs to the most P-rich iron meteorites. In Fig. 5 we compare the INAA data of Twannberg I and II with those of the other four IIG irons on Ga-Au, As-Au and Co-Au diagrams. All four of these elements are useful for distinguishing among iron meteorite groups. The data are consistent with IIG being a group. The two Twannberg points plot close together on all three diagrams; they are very similar in composition to Bellsbank, the latter having a slightly lower Au content. The two Twannberg analyses are resolvably different in their Ir contents (INAA data in Table 3) and may also be different in their Au contents. This difference could be explained by small local differences in the fraction of trapped melt. However, Wasson et al. (2007) noted that Ir and Au values were slightly lower near massive schreibersite in the Santa Luzia iron, so the small differences might also reflect a similar effect caused by solid-state diffusion during cooling.

In group IIAB, Wasson et al. (2007) noted that the skeletal schreibersite and the associated troilite formed from trapped melt. Metal compositions also supported this conclusion. It is probable that IIG schreibersite also formed as a liquidus phase. The size of these crystals increased appreciably as a result of exsolution of P from the cooling taenite, as discussed by Clarke and Goldstein (1978).

It seems possible that the low S contents of IIG irons reflect liquid immiscibility, as discussed for IIAB by Wasson et al. (2007). This explanation would require that S partition very strongly into the S-rich liquid. The low S content could

Table 5. Results of He, Ne, and Ar measurements and cosmogenic components (c). Concentrations in 10^{-8} cm^3 STP/g.

	^{4}He	^{20}Ne	^{40}Ar	^{4}He/^{3}He	^{20}Ne/^{22}Ne	^{22}Ne/^{21}Ne	^{36}Ar/^{38}Ar	^{40}Ar/^{36}Ar	^{4}He$_c$	^{21}Ne$_c$	^{36}Ar$_c$
Twannberg II	41.2	0.153	21.2	4.1	1.22	1.16	0.550	42.1	41.2	0.107	0.50
Sample 35119.2, 98.8 mg	±1.2	±0.013	±0.9	±0.05	±0.06	±0.03	±0.020	±3.5	±1.2	±0.008	0.08
Twannberg I	38.5	0.38	83.4	4.56	0.77	1.33	1.14	160	38.5	0.37	0.26
Sample 56006.3, 103 mg	±1.2	±0.09	±2.5	±0.1	±0.06	±0.13	±0.02	±8	±1.2	±0.10	±0.03
Twannberg I											
Schultz and Franke (2004)	40.0	0.08	1	4.30	0.89	1.00	0.60	3.13	40.0	0.090	0.32

Assumptions for the calculation of the cosmogenic components: $He_{tr} = 0$, $^4He_r = 0$, $(^{20}Ne/^{22}Ne)_c = 0.8$, $(^{20}Ne/^{22}Ne)_{tr} = 9.8$, $(^{21}Ne/^{22}Ne)_{tr} = 0.029$, $(^{36}Ar/^{38}Ar)_{tr} = 5.32$, $(^{36}Ar/^{38}Ar)_c = 0.64$.

Table 6. ^{36}Cl, ^{26}Al, and ^{10}Be activities (dpm/kg) in the Twannberg iron meteorite.

Sample	Mass (mg)	^{36}Cl	^{26}Al	^{10}Be
TW II (T35119/36)	190	0.56 ± 0.09	0.056 ± 0.018	0.108 ± 0.002
TW II (T35119/5)	104	1.0 ± 0.7*(3)	0.076 ± 0.017	0.112 ± 0.005(2)
Wtd average		0.58 ± 0.09	0.066 ± 0.017	0.109 ± 0.002
TW I (T56006/15)	144	0.69 ± 0.08		0.114 ± 0.002
TW I (T56006/6)	143	0.53 ± 0.06 (2)	0.118 ± 0.023	0.112 ± 0.002
TW I (T56006/8)	112	1.15 ± 0.20	0.108 ± 0.023	0.119 ± 0.004
TW I (T56006/9)	104	0.61 ± 0.19 (2)	0.062 ± 0.040	0.119 ± 0.006
Wtd Average		0.59 ± 0.04	0.106 ± 0.015	0.114 ± 0.001

*Uncertainty for 35119/5 is standard deviation of the mean of 3 sample measurements; in all other cases, the uncertainty is calculated from the AMS ratio measurement errors. For 35119/5, the sample-to-sample reproducibility for ^{36}Cl was poor for unknown reasons.

Numbers in parentheses indicate the number of independent analyses made. Typical carrier masses were 1.5 mg for ^{9}Be, 3.0 mg for ^{27}Al, and 25 mg for Cl.

also result if there were minimal amounts of trapped melt. In this case, the high P content might be best understood if schreibersite were a liquidus phase at the time the IIG irons were crystallizing from the melt.

CRE Ages

The CRE ages can be based on the ^{36}Cl-^{36}Ar method as outlined in detail by Lavielle et al. (1999). Chlorine-36 and ^{36}Ar in iron meteorites are produced by spallation reactions with Fe and Ni. Chlorine-36 decays to ^{36}Ar with a branching ratio of 0.981. Since both ^{36}Cl and ^{36}Ar are produced from the same targets and have similar production pathways, their production ratio is almost independent of shielding effects. This circumstance makes them ideal for the calculation of CRE ages. Assuming a constant cosmic ray flux, the ^{36}Cl-^{36}Ar age T_{36} is given by

$$T_{36} = 511 \times P(^{36}Cl)/P(^{36}Ar) \times [^{36}Ar]/[^{36}Cl] \qquad (1)$$

where $P(^{36}Cl)/(P^{36}Ar) = 0.835$ and ^{36}Ar and ^{36}Cl are the ^{36}Ar (10^{-8} cm^3/g) and ^{36}Cl (dpm/kg) concentrations measured in the same sample, respectively.

For Twannberg II an age of 276 Ma is obtained. The Ar data of Twannberg I, sample 56006.3 are not reliable for age dating, considering the high ^{36}Ar/^{38}Ar ratio due to schreibersite inclusions. If the ^{36}Ar value for Twannberg I given in Schultz and Franke (2004) is used, and adopting 0.75 dpm/kg ^{36}Cl, an age of 182 Ma is calculated. CRE ages can also be calculated using the ^{21}Ne-^{10}Be and ^{21}Ne-^{26}Al methods of Lavielle et al. (1999). Assuming that the ^{21}Ne analysis of Twannberg I is affected by schreibersite inclusions, it seems fair to average the ^{21}Ne content for the other two samples (Twannberg II and the data given by Schultz and Francke 2004 for Twannberg I). If one then uses average ^{10}Be and ^{26}Al concentrations, a terrestrial age of ~10 kyr, and equations of Lavielle (1999), one finds a ^{21}Ne-^{10}Be age of 246 Ma and a ^{21}Ne-^{26}Al age of 229 Ma. Thus, an average CRE age for the investigated Twannberg samples of 230 ± 50 Ma is proposed. This age is typical for iron meteorites (Eugster 2003). Their CRE ages are in a range of about 7 Ma for the Rafrüti anomalous ataxite (Terribilini et al. 2000) to about 1000 Ma (cf. Wieler 2002).

Terrestrial Age

The ratios of the ^{36}Cl to the ^{10}Be activities for the six Twannberg samples analyzed yield a value of 6.69 ± 0.96. This ratio can be used to calculate a terrestrial age for Twannberg from the relation

$$\frac{^{36}Cl}{^{10}Be} = \frac{P(^{36}Cl) \times e^{-\lambda_{36} T_{terr}}}{P(^{10}Be) \times e^{-\lambda_{10} T_{terr}}}. \qquad (2)$$

Because ^{36}Cl has a smaller half-life than ^{10}Be, the measured ^{36}Cl/^{10}Be activity ratio is expected to decrease as terrestrial age increases. The production rate ratio, $P(^{36}Cl)/P(^{10}Be)$, is

fairly constant in iron meteorites. For relatively small irons, the ratio P(^{36}Cl)/P(^{10}Be) is ~22/5 = 4.4. As shown in Fig. 4, a line with a slope of 4.4 and passing through the origin fits the experimental data for many iron meteorites reasonably well. For Twannberg, however, the average of the measured ^{36}Cl/^{10}Be activity ratios lies above the trend line. This is a hint that Twannberg was probably large.

Lavielle et al. (1999) made a more detailed study of the ^{36}Cl/^{10}Be production rate ratio. They found that the equation below describes the activities measured in iron meteorites

$$^{36}\text{Cl} = 5.97 \times [^{10}\text{Be}] - 0.184 \times {}^{10}\text{Be}^2 - 0.024 \times [^{10}\text{Be}]^3. \quad (3)$$

For the average ^{10}Be activity of the Twannberg samples, 0.114 dpm/kg, the formula of Lavielle et al. (1999) predict a ^{36}Cl activity (at saturation) of 0.68 dpm/kg and a production rate ratio P(^{36}Cl)/P(^{10}Be) = 5.95.

The measured ^{36}Cl/^{10}Be activity ratio of 6.7 ± 1.0 is somewhat higher than, but agrees within error with, with the expected production rate ratio of 6.0. It is concluded that the terrestrial age of Twannberg is zero within the uncertainties of the calculation (maximum age allowed within error is 28 kyr). Analogous treatment of the ^{26}Al/^{10}Be ratio leads to the same conclusion with a larger uncertainty (maximum age 170 kyr). These values are consistent with a fall during the last glaciation, as indicated with the geological setting.

The activity of ^{36}Cl evidently changed by at most a few percent since the time of fall. The activities of the shorter-lived cosmogenic radionuclides ^{41}Ca or ^{14}C would have changed by larger percentages and could therefore provide better estimates of Twannberg's terrestrial age. The measurements would be difficult however, as production rates in the samples of Twannberg analyzed so far were quite low.

Shielding and Preatmospheric Size

Excluding the cosmogenic ^{21}Ne concentration of Twannberg I, sample 56006.3 (schreibersite inclusions, see above), an average ^{21}Ne production rate, P(^{21}Ne), of 0.043 × 10^{-10} cm^3 STP/g·Ma is calculated from the data in Table 5 and a CRE age of 230 ± 50 Ma. Furthermore, a cosmogenic ratio ^{4}He/^{21}Ne of 415 is obtained. With these data for P(^{21}Ne) and ^{4}Ne/^{21}Ne, Twannberg plots in the lower right hand corner of Fig. 7 of Voshage and Feldmann (1979), close to Anoka and several other irons thought to have been very large in space.

Some additional information about the sample locations and meteoroid size can be obtained by comparing measured and modeled radionuclide activities. Michlovich et al. (1994) presented modeling calculations for Canyon Diablo, which although likely much larger than Twannberg, provides a rough guide for comparison. Their Figs. 1–4 (LAHET code particle fluxes) indicate that the activities measured in Twannberg correspond to the following shielding depths ^{36}Cl, 68 cm; ^{26}Al, 69; ^{10}Be, 63 cm. Calculations for a smaller body might increase these estimates of depth slightly. A radius of 69 cm implies a minimum mass of 11,000 kg for a spherical object with a density of 8 g/cm^3. Given the fact that TW I and TW II are derived from a similar depth, it may be speculated that these masses were derived from the same individual due to breakup during terrestrial residence. Arguments for such speculations are missing, however.

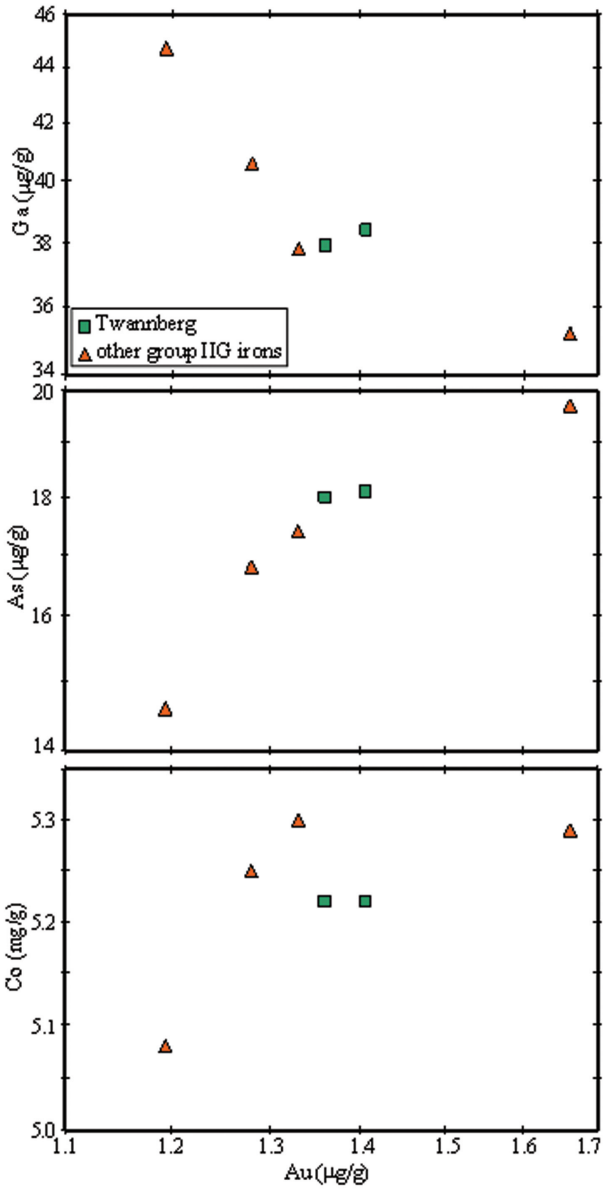

Fig. 5. Comparison of INAA data of Twannberg I and II with INAA analyses of the other four IIG irons (J. T. Wasson, unpublished data). The IIG iron with similar composition and a slightly lower Au content is Bellsbank.

CONCLUSIONS

The similarity of the meteoritic iron masses I and II recovered in the Twannberg area in terms of chemical

composition, structure, mineralogy, alteration history, noble gas concentrations, CRE ages, and concentrations of cosmogenic radioisotopes demonstrate without doubt that they are paired. The similarity of TW III–VI to TW I and II are also numerous: skeletal schreibersite of unusual size, high bulk P based on schreibersite mode, and the adhesion of local glacial till material (quite uncommon in iron meteorites) demonstrate pairing as well.

The indication of a large preatmospheric mass of about 10,000 kg and the independent discovery of six fragments indicate that very likely more fragments are present in the area. The high abundance of brittle schreibersite may have facilitated breakup during atmospheric entry. The CRE age of Twannberg (about 230 Ma) is within the range typically observed for iron meteorites.

Abundant quartz grains and rock fragments present in the alteration rinds of the three large masses indicate intimate contact with glacial till material of the Rhône glacier during weathering. It appears possible, therefore, that the meteorites were transported by the Rhône glacier during the Würm ice age and the actual place of fall might be anywhere in the large catchment area (up to 150 km upstream). Other fragments of this fall might be scattered over a very large area, therefore, and are most likely to be found in areas covered by till of the Rhône glacier.

Acknowledgments—The finders Margrit Christen, Marc Jost, Marcel Wälti, and Daniel Ducrest are gratefully acknowledged for their cooperation and help in providing information about their finds. The friends of the museum (Museumsverein) of the Natural History Museum Bern provided the funds for the acquisition of masses I and II from the Conrad und Mariette Burri-Kircheisen Fund. The Naturschutzinspektorat des Kantons Bern provided funds for field search with a metal detector. Various informations were kindly provided by Pascal Monnerat and Rolf W. Bühler. Reviewers Joe Goldstein, Henning Haack, and Kees Welten helped to significantly improve the manuscript.

Editorial Handling—Dr. Nancy Chabot

REFERENCES

Buchwald V. F. 1975. *Handbook of iron meteorites*. Berkeley: University of California Press. 1418 p.

Bühler R. W. 1986a. Der Eisenmeteorit Twannberg. *Neue Zürcher Zeitung*, November 12, 1986, p. 65.

Bühler R. W. 1986b. Twannberg—ein neuer Schweizer Eisenmeteorit. *Orion* 217:188–192.

Bühler R. W. 1988. *Meteorite: Urmaterie aus dem interplanetaren Raum*. Basel: Birkhäuser. 192 p.

Clarke R. S. and Goldstein J. I. 1978. Schreibersite growth and its influence on the metallography of coarse-structured iron meteorites. *Smithsonian Contributions to the Earth Sciences* 21: 1–80.

Doan A. S. and Goldstein J. I. 1969. The formation of phosphides in iron meteorites. In *Meteorite research*, edited by Millman P. M. Berlin: Springer. pp. 763–779.

Eugster O. 2003. Cosmic-ray exposure ages of meteorites and lunar rocks and their significance. *Chemie der Erde/Geochemistry* 63: 3–30.

Eugster O., Michel T., Niedermann S., Wang D., and Yi W. 1993. The record of cosmogenic, radiogenic, fissiogenic, and trapped noble gases in recently recovered Chinese and other chondrites. *Geochimica et Cosmochimica Acta* 57:1115–1142.

Geist V., Wagner G., Nolze G., and Moretzki O. 2005. Investigations of the meteoritic mineral $(Fe,Ni)_3P$. *Crystal Research and Technology* 40:52–64.

Grady M. M. 2000. *Catalogue of meteorites*, 5th ed. Cambridge: Cambridge University Press. 696 p.

Graham A. L. 1986. The Meteoritical Bulletin, No. 64. *Meteoritics & Planetary Science* 21:309–313.

Hofmann B. A. 2005. Die Twannberg-Eisenmeteoriten. *Schweizer Strahler* 39:26–32.

Jäckli H. 1970. Atlas der Schweiz. Die Schweiz zur letzten Eiszeit. Eidgenössische Landestopographie, Wabern-Bern.

Lavielle B., Marti K., Jeannot J.-P., Nishiizumi K., and Caffee M. 1999. The ^{36}Cl-^{36}Ar-^{40}K-^{41}K records and cosmic ray production rates in iron meteorites. *Earth and Planetary Science Letters* 170: 93–104.

Michlovich E. S., Vogt S., Masarik J., Reedy R. C., Elmore D., and Lipschutz M. E. 1994. Aluminum 26, ^{10}Be, and ^{36}Cl depth profiles in the Canyon Diablo iron meteorite. *Journal of Geophysical Research* 99(E11):23,187–23,194.

Nishiizumi K., Klein J., Middleton R., and Arnold J. R. 1987. Long-lived cosmogenic nuclides in the Derrick Peak and Lazarev iron meteorites. 28th Lunar and Planetary Science Conference. pp. 725–726.

Randich E. and Goldstein J. I. 1978. Cooling rates of seven hexahedrites. *Geochimica et Cosmochimica Acta* 42:221–233.

Russell S. S., Folco L., Grady M. M., Zolensky M. E., Jones R. H., Righter K., Zipfel J., and Grossman J. N. 2004. The Meteoritical Bulletin, No. 88. *Meteoritics & Planetary Science* 39:A215–A272.

Schär U., Ryniker K., Schmid K., Häfeli C., and Rutsch R. F. 1971. Blatt 1145 Bieler See. In *Geologischer Atlas der Schweiz 1: 25,000*, edited by Kommission S. G. Bern: Kümmerli & Frey.

Schultz L. and Franke L. 2004. Helium, neon and argon in meteorites: A data compilation. *Meteoritics & Planetary Science* 39:1889–1890, Online appendix at http://meteoritics.org/Online%20Supplements.htm.

Terribilini D., Eugster O., Mittlefehldt D. W., Diamond L.W., Vogt S. and Wang D. 2000. Mineralogical and chemical composition and cosmic-ray exposure history of two mesosiderites and two iron meteorites. *Meteoritics & Planetary Science* 35:617–628.

Vogt S. and Herpers U. 1988. Radiochemical separation techniques for the determination of long-lived radionuclides in meteorites by means of accelerator mass spectrometry. *Fresenius Zeitschrift für Analytische Chemie* 331:186–188.

Vogt S., Wang M.-S., Li R., and Lipschutz M. 1994. Chemistry operations at Purdue's accelerator mass spectrometry facility. *Nuclear Instruments and Methods in Physics Research B* 92: 153–157.

Voshage H. and Feldmann H. 1979. Investigations of cosmic-ray-produced nuclides in iron meteorites, 3: Exposure ages, meteoroid sizes and sample depths determined by spectrometric analyses of potassium and rare gases. *Earth and Planetary Science Letters* 45:293–308.

Wasson J. T. and Choi B.-G. 2004. Main-group pallasites: Chemical composition, relationship to IIIAB irons, and origin. *Geochimica et Cosmochimica Acta* 67:3079–3096.

Wasson J. T., Huber H. J., and Malvin D. J. 2007. Formation of IIAB iron meteorites. *Geochimica et Cosmochimica Acta* 71:760–781.

Wasson J. T., Ouyang X., Wang J., and Jerde E. 1989. Chemical classification of iron meteorites: XI. Multi-element studies of 38 new irons and the high abundance of ungrouped irons from Antarctica. *Geochimica et Cosmochimica Acta* 53:735–744.

Wieler R. 2002. Cosmic-ray-produced noble gases in meteorites. In *Noble gases in geochemistry and cosmochemistry*, edited by Porcelli D., Ballantine C. J. and Wieler R. Reviews in Mineralogy and Geochemistry, vol. 47. Washington, D.C.: Mineralogical Society of America. pp. 125–170.

Xue S., Herzog G. F., Souis A., Ervin M. H., Lareau R. T., Middleton R., and Klein J. 1995. Stable magnesium isotopes, ^{26}Al, ^{10}Be, and ^{26}Mg/(^{26}Al) exposure ages of iron meteorites. *Earth and Planetary Science Letters* 136:397–406.